JOURNAL OF ELECTROMAGNETIC ENGINEERING AND SCIENCE, VOL. 18, NO. 1, 1~6, JAN. 2018

https://doi.org/10.26866/jees.2018.18.1.1
ISSN 2234-8395 (Online) · ISSN 2234-8409 (Print)

Resonance Frequency and Bandwidth of the Negative/Positive n^{th} Mode of a Composite Right-/Left-Handed Transmission Line

Seong-Jung Kim · Jeong-Hae Lee*

Abstract

In this study, the analytic expression for the positive/negative n^{th}-mode resonance frequency of an N unit cell composite right-/left-handed (CRLH) transmission line is derived. To explain the resonance mechanism of the n^{th} mode, especially for the negative mode, the current distribution of the N unit cell CRLH transmission line is investigated with a circuit simulation. Results show that both positive and negative n^{th} resonance modes have n times current variations, but their phase difference is 180° as expected. Moreover, the positive n^{th} resonance occurs at a high frequency, whereas the negative n^{th} resonance transpires at a low frequency, thus indicating that the negative resonance mode can be utilized for a small resonator. The correlation between the slope of the dispersion curve and the bandwidth is also observed. In sum, the balanced condition of the CRLH transmission line provides a broader bandwidth than the unbalanced condition.

Key Words: Bandwidth, Composite Right-/Left-Handed Transmission Line, Field Distribution, $\pm n^{th}$-Mode Resonance Frequency.

I. INTRODUCTION

Electromagnetic metamaterials (MTMs) [1] are broadly defined as artificial and effectively homogeneous electromagnetic structures with unusual properties not readily available in nature. MTMs enable the generation of left-handed waves through effective negative permittivity and permeability. MTMs have various applications, such as lens, absorber, and cloak, among others [2–4].

However, MTMs have a limitation when applied to radio frequency (RF) devices because they are lossy and have a narrow bandwidth (BW) in the microwave frequency range. To overcome these problems, the composite right-/left-handed (CRLH) transmission line (TL) was introduced [5]. Many miniaturized antennas, power dividers, resonators, filters, and couplers [6–12] can be designed and applied for many RF applications using CRLH TLs. However, until now, no detailed investigation on the positive/negative n^{th}-mode resonance frequency and its BW of N unit cell CRLH TL has been conducted as far as we know.

This study defines the negative mode and provides the guideline for designing a resonance antenna using the CRLH TL. The physical resonance mechanism can be explained by using the circuit model. Specifically, the difference between the negative and positive modes can be clearly seen, and the physical meaning of the negative mode is explained. Moreover, by deriving the analytic expression of the negative/positive n^{th} mode resonance frequency to show the correlation between

Manuscript received August 10, 2017 ; Revised October 18, 2017 ; Accepted November 6, 2017. (ID No. 20170810-035J)
School of Electronic and Electrical Engineering, Hongik University, Seoul, Korea.
*Corresponding Author: Jeong-Hae Lee (e-mail: jeonglee@hongik.ac.kr)

the BW and the dispersion curve slope, this study provides the guideline for easily designing a resonance antenna.

II. Resonance Mechanism of the Negative/Positive nth Mode of the N Unit Cell CRLH TL

Fig. 1 shows the current distribution of the positive/negative n^{th} mode for N cells with an open boundary condition at both ends. For the n^{th} mode, because the total electrical length is a multiple of π with an open-ended boundary, the $n\pi/N$ phase delay is expected to occur per unit cell when $n = 0, \pm 1, \cdots, \pm N-1$, and the current distribution has n time variations of a standing wave pattern for both the positive and negative modes. The length of one variation corresponds to a half wavelength of each mode. Therefore, both the n^{th} positive and negative modes have the same wavelength (or the same magnitude of a propagation constant) even though the corresponding frequencies are different because of different dispersion branches. However, the phase difference between the positive and the negative mode is 180° because of the opposite direction of the propagation direction between the two modes. The phase difference of 180° is easy to understand from the current standing wave pattern with an open boundary condition at both ends given by

$$I = I_0^+(e^{-j\beta z} - e^{+j\beta z}) = -2jI_0^+ \sin\beta z\,, \quad (1)$$

$$I = I_0^+(e^{+j\beta z} - e^{-j\beta z}) = +2jI_0^+ \sin\beta z\,, \quad (2)$$

where (1) and (2) are the positive mode and the negative mode, respectively.

To confirm the illustration in Fig. 1, the current distribution of the N unit cell CRLH TL with an open boundary condition is simulated with the Advanced Design System (Fig. 2). If a lossless structure with no resistance exists, only the magnitude of the reactance will distribute the amplitude of the current and the voltage. For $N = 3$, the voltages and the currents of each node in Fig. 2 are measured with probes labeled $P_{0,1,2,} \cdots, N$ and compared (Fig. 3).

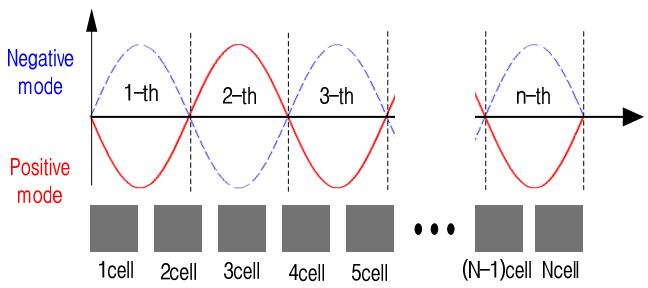

Fig. 1. Current distribution of the positive/negative n^{th} mode for N cells with an open boundary condition.

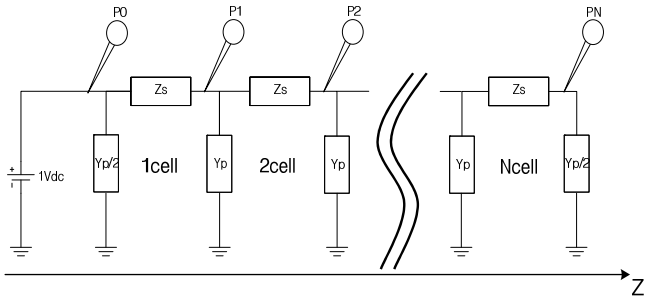

$$(Z_S = \omega L_R - \frac{1}{\omega C_L},\ Y_P = \omega C_R - \frac{1}{\omega L_L},\ L_R = 13.7nH,$$
$$C_L = 0.18pF, L_L = 1.58nH,\ C_R = 1.97pF)$$

Fig. 2. Equivalent CRLH circuit with an open boundary condition at both ends.

The magnitude of the voltage and the current is normalized to 1, and the current flowing in the -z direction is a (+) sign. The left column of Fig. 3 shows the positive modes and the right column shows the negative modes. The result indicates that the voltage and the current have a cosine and sine distribution, respectively, except for the 0^{th} mode.

For the 0^{th} mode, no current flows and the voltage operates without a phase delay because of the zero value of Y_p. The 0^{th}-order resonance with an open-ended boundary condition occurs at the shunt resonance ($Y_p = 0$). Moreover, the number of half wavelength variations increases as the mode number of n increases. When the distributions of the positive and negative modes are compared, note that the current distribution changes to 180° in the phase as discussed previously, and the voltage distribution is the same as that in the open boundary condition.

In terms of the circuit, the P_0 probe is fixed at +1 Vdc at the input node. Therefore, its amplitude is +1 V regardless of the mode. For the positive mode, $Y_p/2$ has a positive value because C_R is predominant over L_L; for the negative mode, $Y_p/2$ has a negative value because L_L is predominant over C_R. Therefore, the direction of the current changes in the negative mode. The reason for the existence of negative modes is that they are another combination that makes the total input reactance zero. In other words, Z_s and Y_p of the negative mode have the same ratio as Z_s and Y_p of the positive mode. The only difference is that the signs of $\mathrm{Im}(Z_s)$ and $\mathrm{Im}(Y_p)$ of the negative mode are negative and those of $\mathrm{Im}(Z_s)$ and $\mathrm{Im}(Y_p)$ of the positive mode are positive. Fig. 3 satisfies the condition of $1/\sqrt{L_L C_R} > 1/\sqrt{L_R C_L}$ with an open boundary condition. In this case, it has a positive mode when the angular frequency is larger than the shunt angular resonance frequency of $1/\sqrt{L_L C_R}$. Conversely, it has a negative mode when it is smaller than $1/\sqrt{L_R C_L}$. Similarly, if it is a short boundary condition, the 0^{th}-order mode angular frequency is given by the series resonance of $1/\sqrt{L_R C_L}$. In addition, the vol-

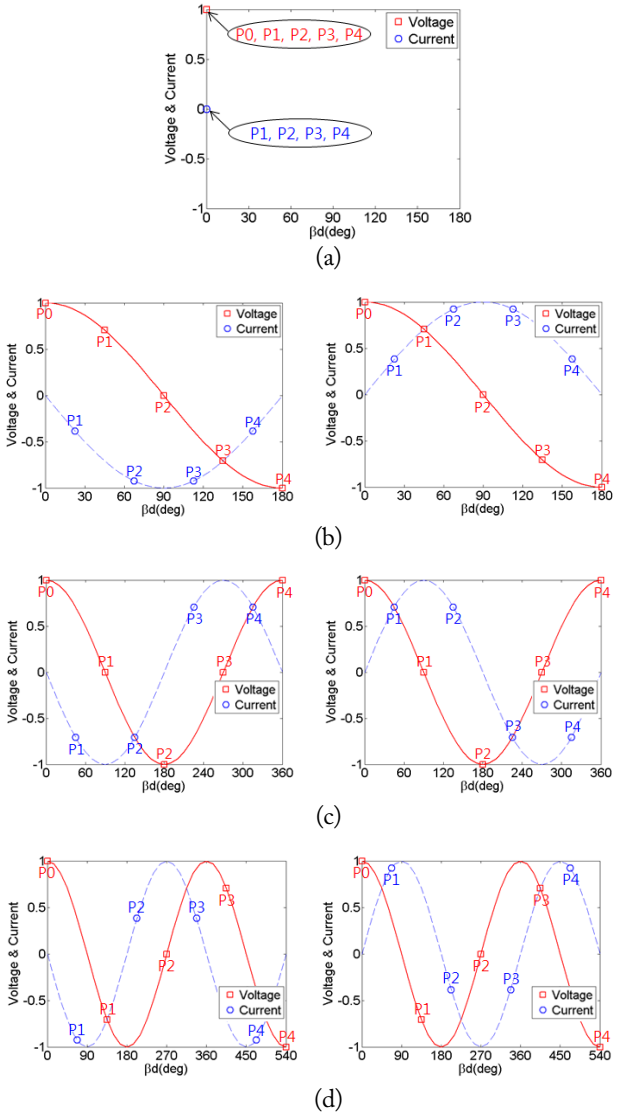

Fig. 3. Results of the voltages and the currents of each node. (a) 0[th] mode, (b) +1[th] mode and -1[th] mode, (c) +2[th] mode and -2[th] mode, (d) +3[th] mode and -3[th] mode.

tage follows the sine distribution, and the current follows the cosine distribution. The phases of the positive and negative mode currents are also 180° apart from each other.

III. Derivation of Resonance Frequency

The unit cell of CRLH TL can be drawn as an equivalent T circuit as shown in Fig. 4.

The following relation can be obtained by using the phase difference ($\theta = n\pi/N$) between two terminals:

$$V_n = V_{n+1} e^{j\theta}$$
$$I_n = I_{n+1} e^{j\theta} \quad , \tag{3}$$

where N is the number of total unit cells, and n is the number of

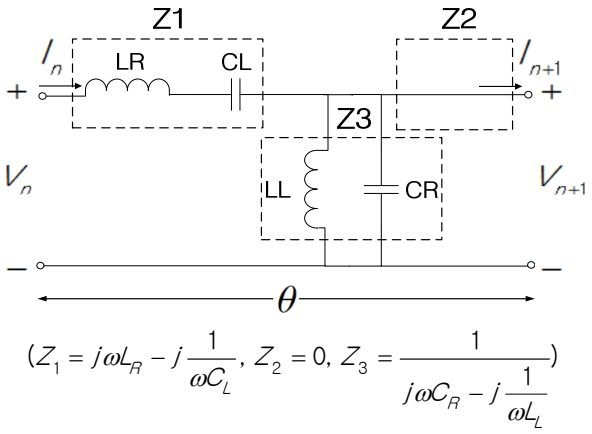

Fig. 4. Equivalent circuit of a CRLH unit cell.

arbitrary unit cells.

Eq. (3) is represented by a matrix. When it is compared with the ABCD matrix, the following equation is obtained:

$$\begin{bmatrix} A - e^{j\theta} & B \\ C & D - e^{j\theta} \end{bmatrix} \begin{bmatrix} V_{n+1} \\ I_{n+1} \end{bmatrix} = O \,. \tag{4}$$

As Eq. (4) has a non-trivial solution and the circuit in Fig. 4 is reciprocal ($AD - BC = 1$), we can summarize both as Eq. (5):

$$1 - e^{j\theta}(A + D) + e^{j2\theta} = O \,, \tag{5}$$

where

$$A = 1 + (j\omega L_R - j\frac{1}{\omega C_L})(j\omega C_R - j\frac{1}{\omega L_L}), \quad D = 1 \,.$$

Eq. (5) is a quartic equation for ω. By substitution into a quadratic equation, the following equation can be obtained:

$$\omega = \sqrt{\frac{\omega_E^2 + \omega_M^2 + 2\omega_R^2(1-\cos\theta) \pm \sqrt{(\omega_E^2 + \omega_M^2 + 2\omega_R^2(1-\cos\theta))^2 - 4\omega_L^2\omega_R^2}}{2}} \tag{6}$$

where

$$\omega_R = \frac{1}{\sqrt{L_R C_R}}, \ \omega_L = \frac{1}{\sqrt{L_L C_L}}, \ \omega_E = \frac{1}{\sqrt{L_L C_R}}, \ \omega_M = \frac{1}{\sqrt{L_R C_L}}$$

To confirm the result of Eq. (6), the resonance frequencies of the three-unit cell CRLH TL are calculated using the circuit simulation of Ansoft Designer and the full wave simulation of HFSS. Fig. 5 is the electrically coupled three-unit cell CRLH equivalent circuit employed in the circuit simulation. Fig. 6 shows the mushroom structure, and Fig. 5 illustrates its parameters (C_R, L_R, C_L, and L_L) and their values. The structure in Fig. 6 is obtained from [13] and simulated by High Frequency Structure Simulator (HFSS). Table 1 compares the resonance frequencies of the three-unit cell CRLH TL obtained from Eq. (6),

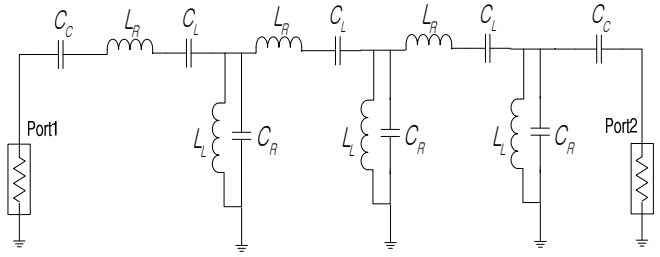

Fig. 5. Structure fed via electrical coupling (N=3 using the Ansoft Designer circuit tool). C_c =0.1 pF, L_R=13.7 nH, C_L =0.18 pF, L_L =1.58 nH, C_R=1.97 pF.

Table 1. Comparison of resonance frequencies of N=3 CRLH TL with an open boundary (unit: GHz)

	-2^{th} mode	-1^{th} mode	0^{th} mode	$+1^{th}$ mode	$+2^{th}$ mode
Eq. (6)	2.29	2.55	2.85	3.58	4.00
Circuit	2.28	2.52	2.81	3.55	3.98
HFSS	2.71	2.88	3.16	3.59	3.94

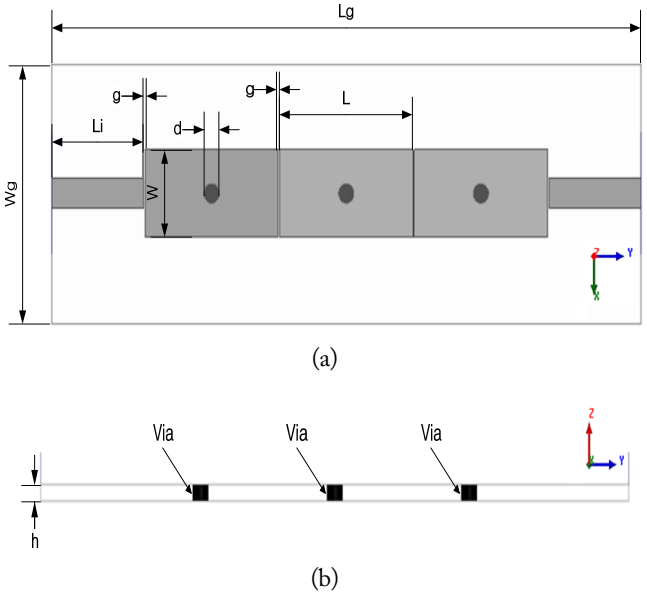

Fig. 6. Schematic of the proposed three-cell CRLH mushroom resonant antenna: (a) top view and (b) side view. L_g=90 mm, W_g=30 mm, L_i=13.8 mm, W_i=3.5 mm, L=20 mm, W=10 mm, d=2.4 mm, g=0.2 mm (Rogers RO-4003 substrate with thickness h=1.524 mm and dielectric constant of 3.55).

HFSS, and Ansoft Designer, respectively.

Table 1 shows that the results obtained by Eq. (6), and all the data in Table 1 are obtained with an unbalanced condition. The circuit simulation is almost the same as expected. However, the results from HFSS have some differences in the resonance frequencies caused by the errors of the extracted parameters (C_R, L_R, C_L, and L_L) from the real structure. The method of parameter extraction from the dispersion curve inevitably cannot produce perfect matched results in all modes. However, the overall results are in good agreement.

IV. Correlation between Slope and BW

The slope of the dispersion curve $df/d\theta$ (θ = electrical length per unit cell) is a measure of how much the frequency changes as the electrical length changes. The higher the slope is, the greater the frequency changes even with a change in electrical length. In other words, a large value of $\frac{1}{d\theta/df}$ means that the electrical length changes insensitively even when the frequency changes greatly. In a resonator, resonance depends on the electrical length because it occurs when the electrical length is an integer multiple of a half wavelength. Therefore, the slope of the dispersion curve correlates with the BW. The BW is defined as S_{11} <–10 dB, and the slope is calculated by differentiating the dispersion curve with the equation of $df/d\theta$. Tables 2 and 3 show the correlation between slope and BW for various cells and modes according to an unbalanced or a balanced condition [5]. The correlation coefficient is defined as

$$\rho = \frac{\sum (x-\bar{x})(y-\bar{y})}{\sqrt{\sum (x-\bar{x})^2 \times \sum (y-\bar{y})^2}}$$
$$\rho : \textit{correlation coefficient}$$
$$x : \textit{bandwidth of each modes}$$
$$y : \textit{slope of dispersion curve} \quad (7)$$

In Tables 2 and 3, the dimensions of slope and BW are in MHz/° and MHz, respectively. Except for the 0^{th} mode of the unbalanced condition, Tables 2 and 3 show that the slope is always closely related to the BW. Fig. 7 illustrates that the BW, which is correlated with the dispersion curve slope, is significantly improved when the balanced condition is satisfied [14]. In other words, the overall BW improves because the average slope from 0° to 180° increases from 5.3 MHz/° to 25.3 MHz/°. This finding can be confirmed by comparing Tables 2 and 3.

V. Conclusion

This study has successfully derived the analytic expression for the positive/negative n^{th}-mode resonance frequency of an N unit cell CRLH transmission line. The resonance mechanism of the n^{th} positive/negative mode is investigated by the current distribution of an N unit cell CRLH transmission line. Both the positive and the negative n^{th} resonance modes have n times current variation, but their phase difference is 180°. The slope of the CRLH dispersion curve is closely correlated with the BW. When the CRLH TL is designed with a balanced condition,

Table 2. Correlation coefficient between BW and slope in an unbalanced condition

# of cells		-4^{th} mode	-3^{th} mode	-2^{th} mode	-1^{th} mode	0^{th} mode	$+1^{th}$ mode	$+2^{th}$ mode	$+3^{th}$ mode	$+4^{th}$ mode	Correlation coefficient
N=3	Slope (MHz/°)	-	-	3.01	5.73	-	8.04	5.27	-	-	0.990
	BW (MHz)	-	-	1.13	4.92	6.89	7.74	4.94	-	-	
N=4	Slope (MHz/°)	-	2.26	4.47	6.11	-	8.00	7.11	4.09	-	0.956
	BW (MHz)	-	0.46	2.02	4.90	5.16	5.18	5.61	2.32	-	
N=5	Slope (MHz/°)	1.81	3.60	5.27	6.14	-	7.72	7.80	6.09	3.33	0.932
	BW (MHz)	0.31	1.30	2.52	4.65	4.02	3.43	4.80	3.60	1.19	

C_c=0.1 pF, L_R=13.7 nH, C_L=0.18 pF, L_L=1.58 nH, C_R=1.97 pF.

Table 3. Correlation coefficient between BW and slope in a balanced condition

# of cells		-4^{th} mode	-3^{th} mode	-2^{th} mode	-1^{th} mode	0^{th} mode	$+1^{th}$ mode	$+2^{th}$ mode	$+3^{th}$ mode	$+4^{th}$ mode	Correlation coefficient
N=3	Slope (MHz/°)	-	-	4.48	13.40	27.97	35.06	23.14	-	-	0.919
	BW (MHz)	-	-	35.30	172.0	407.4	426.9	156.5	-	-	
N=4	Slope (MHz/°)	-	3.44	8.36	16.61	27.97	35.07	31.20	17.97	-	0.928
	BW (MHz)	-	14.0	64.5	169.1	306.0	346.6	228.6	69.30	-	
N=5	Slope (MHz/°)	2.69	6.10	11.16	18.85	27.97	34.45	34.09	26.78	14.60	0.932
	BW (MHz)	6.90	30.70	78.70	156.8	245.0	282.5	232.2	129.1	36.20	

C_c=5 pF, L_R=13.7 nH, C_L=0.18 pF, L_L=13.7 nH, C_R=0.18 pF.

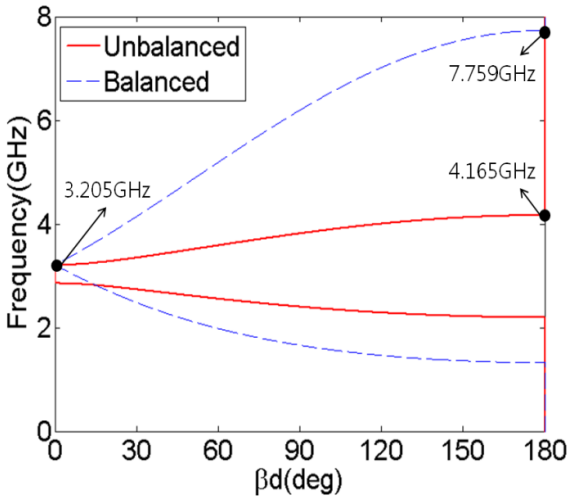

Fig. 7. Dispersion curves of slope and BW in Tables 2 and 3.

the BW increases from the slope.

This research was supported by the Basic Science Research Program through the National Research Foundation of Korea (NRF) funded by the Ministry of Education (No. 2015-R1A6A1A03031833) and the Ministry of Science and ICT, Korea, under the Information Technology Research Center support program (No. IITP-2017-2016-0-00291), which is supervised by the Institute for Information & Communications Technology Promotion.

REFERENCES

[1] V. G. Veselago, "The electrodynamics of substances with si-

multaneously negative values of and μ," *Soviet Physics Uspekhi*, vol. 10, no. 4, pp. 509–514, 1968.
[2] D. Schurig, J. J. Mock, B. J. Justice, S. A. Cummer, J. B. Pendry, A. F. Starr, and D. R. Smith, "Metamaterial electromagnetic cloak at microwave frequencies," *Science*, vol. 314, no. 5801, pp. 977–980, 2006.
[3] J. B. Pendry, "Negative refraction makes a perfect lens," *Physical Review Letters*, vol. 85, no. 18, pp. 3966–3969, 2000.
[4] N. I. Landy, S. Sajuyigbe, J. J. Mock, D. R. Smith, and W. J. Padilla, "Perfect metamaterial absorber," *Physical Review Letters*, vol. 100, no. 20, article no. 207402, 2008.
[5] A. Sanada, C. Caloz, and T. Itoh, "Characteristics of the composite right/left-handed transmission lines," *IEEE Microwave and Wireless Components Letters*, vol. 14, no. 2, pp. 68–70, 2004.
[6] J. H. Park, Y. H. Ryu, J. G. Lee, and J. H. Lee, "Epsilon negative zeroth-order resonator antenna," *IEEE Transactions on Antennas and Propagation*, vol. 55, no. 12, pp. 3710–3712, 2007.
[7] A. Genc and R. Baktur, "Dual-and triple-band Wilkinson power dividers based on composite right-and left-handed transmission lines," *IEEE Transactions on Components, Packaging and Manufacturing Technology*, vol. 1, no. 3, pp. 327–334, 2011.
[8] C. A. Allen, K. M. K. H. Leong, and T. Itoh, "Design of microstrip resonators using balanced and unbalanced composite right/left-handed transmission lines," *IEEE Transactions on Microwave Theory and Techniques*, vol. 54, no. 7, pp. 3104–3112, 2006.
[9] G. Kim and B. Lee, "Synthesis of bulk medium with negative permeability using ring resonators," *Journal of Electromagnetic Engineering and Science*, vol. 16, no. 2, pp. 67–73, 2016.
[10] J. Y. Lee, D. J. Kim, and J. H. Lee, "High order bandpass filter using the first negative resonant mode of composite right/left-handed transmission line," *Microwave and Optical Technology Letters*, vol. 51, no. 5, pp. 1182–1185, 2009.
[11] J. Jeon, S. Kahng, and H. Kim, "GA-optimized compact broadband CRLH band-pass filter using stub-inserted interdigital coupled lines," *Journal of Electromagnetic Engineering and Science*, vol. 15, no. 1, pp. 31–36, 2015.
[12] C. Caloz, A. Sanada, and T. Itoh, "A novel composite right-/left-handed coupled-line directional coupler with arbitrary coupling level and broad bandwidth," *IEEE Transactions on Microwave Theory and Techniques*, vol. 52, no. 3, pp. 980–992, 2004.
[13] N. Amani and A. Jafargholi, "Zeroth-order and TM_{10} modes in one-unit cell CRLH mushroom resonator," *IEEE Antennas and Wireless Propagation Letters*, vol. 14, pp. 1396–1399, 2015.
[14] l, J. Bonache, J. Selga, J. Garcia-Garcia, and F. Martin, "Broadband resonant-type metamaterial transmission lines," *IEEE Microwave and Wireless Components Letters*, vol. 17, no. 2, pp. 97–99, 2007.

Seong-Jung Kim

received his B.S. degree in electronic and electrical engineering from Hongik University, Seoul, Korea, in 2017. He is currently working toward an integrated master's and Ph.D. degree in the Department of Electrical and Information Engineering at Seoul National University, Seoul, Korea. His main research interests are metamaterial transmission lines and antennas.

Jeong-Hae Lee

received his B.S. and M.S. degrees in electrical engineering from Seoul National University, Korea, respectively, and his Ph.D. degree in electrical engineering from the University of California, Los Angeles, CA, USA. He was a visiting scientist of General Atomics, San Diego, CA, where his major research was to develop the millimeter-wave diagnostic system and plasma wave propagation. Since 1996, he has been with Hongik University, Seoul, Korea, where he is a professor of the Department of Electronic and Electrical Engineering. He has more than 100 journal papers and 60 patents. He is currently the vice president of the Korea Institute of Electromagnetic Engineering and Science and the director of the Metamaterial Electronic Device Center. His current research interests include metamaterial/metasurface RF devices and wireless power transfer.